J. Phys.: Condens. Matter **21** (2009) 016005 (6pp) doi:10.1088/0953-8984/21/1/016005

Spin waves in antiferromagnetically coupled bimetallic oxalates

Peter L Reis[1,2] **and Randy S Fishman**[2]

[1] Physics Department, University of North Dakota, Grand Forks, ND 58202-7129, USA
[2] Materials Science and Technology Division, Oak Ridge National Laboratory, Oak Ridge, TN 37831-6065, USA

Received 4 September 2008, in final form 11 September 2008
Published 2 December 2008
Online at stacks.iop.org/JPhysCM/21/016005

Abstract
Bimetallic oxalates are molecule-based magnets with transition-metal ions M(II) and M′(III) arranged on an open honeycomb lattice. Performing a Holstein–Primakoff expansion, we obtain the spin-wave spectrum of antiferromagnetically coupled bimetallic oxalates as a function of the crystal-field angular momentum L_2 and L_3 on the M(II) and M′(III) sites. Our results are applied to the Fe(II)Mn(III), Ni(II)Mn(III) and V(II)V(III) bimetallic oxalates, where the spin-wave gap varies from 0 meV for quenched angular momentum to as high as 15 meV. The presence or absence of magnetic compensation appears to have no effect on the spin-wave gap.

(Some figures in this article are in colour only in the electronic version)

1. Introduction

Bimetallic oxalates have been the subject of intense experimental research since they were first synthesized in 1992 [1]. Within each bimetallic layer, transition-metal ions M(II) and M′(III) are coupled by oxalate molecules ox $= C_2O_4$ on the open honeycomb lattice sketched in figure 1 with nearest-neighbor separation $a \approx 5.4$ Å [2, 3]. The chemical formula for bimetallic oxalates is A[M(II)M′(III)$(ox)_3$], where A is an organic cation that separates the bimetallic layers. For different transition-metal ions, bimetallic oxalates can magnetically order as ferrimagnets, antiferromagnets or ferromagnets [4–7] with moments pointing out-of-the-plane. The cation A lying between the layers does not change the sign of the exchange between the M(II) and M′(III) moments but can influence the optical and metallic properties of the bimetallic oxalates [8]. Recent theoretical calculations [9–11] used a simple model to explain many of the magnetic properties of these materials. We now extend those calculations to evaluate the spin-wave (SW) spectrum of antiferromagnetically coupled bimetallic oxalates.

Evidence that cation A is not responsible for the magnetic order of bimetallic oxalates was found in the Fe(II)Fe(III) family, where it was observed that even compounds with well-separated bimetallic layers can have high transition temperatures [4]. Additional support stems from the observation that a radical spin-1/2 cation does not appreciably change the transition temperature and coercive field [3],

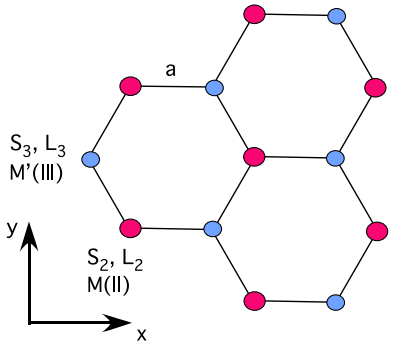

Figure 1. The open honeycomb lattice showing the alternating M(II) and M′(III) sites. L_2 and L_3 are the crystal-field orbital angular momenta on each site.

suggesting that the bimetallic planes are weakly coupled. Earlier work [9, 10] argued that the magnetic properties of the bimetallic oxalates are controlled by the spin–orbit coupling, which can stabilize magnetic order within an isolated layer.

When the exchange interaction between the M(II) and M′(III) moments is antiferromagnetic, it is possible for the sublattice magnetizations to exactly cancel at a compensation temperature T_{comp} below the transition temperature T_c. Magnetic compensation (MC) has been observed in the Fe(II)Fe(III) compounds only for certain cations A [4]. Compounds that exhibit MC also possessed the highest values of T_c and Curie–Weiss constant C [4]. Fishman and Reboredo [9, 10] suggested that MC occurs when the orbital

angular momentum of the low-lying crystal-field doublet on the Fe(II) sites exceeds a threshold value. To determine if other bimetallic oxalates could also exhibit MC for certain cations, we included spin–orbit coupling on both the M(II) and M′(III) sites [11]. MC was found to be possible in the M(II)Mn(III) (M = Fe, Co or Ni) and V(II)M′(III) (M′ = Cr or V) families. Spin–orbit anisotropy is also expected to generate a gap in the SW spectrum. So it is natural to wonder if there is any connection between the presence of MC and the magnitude of the SW gap.

This paper is divided into five sections. Section 2 discusses the important energy scales in the bimetallic oxalates. Section 3 briefly explains how we calculate the magnetization of a bimetallic layer including spin–orbit coupling on both sublattices. The SW spectrum of an antiferromagnetically coupled bimetallic oxalate is derived in section 4. A conclusion appears in section 5.

2. Crystal field

Bimetallic oxalates are characterized by three different energy scales. Since the spin correlations within the 3d orbitals are large, Hund's first rule is obeyed [3]. Measurements of the magnetic susceptibility χ, magnetic moment and Curie constant C of the bimetallic oxalates all confirm that the 3d ions are found in their high-spin states [4, 6]. The C_3-symmetric crystal-field potential produced by the six oxygen atoms surrounding each ion is the next-highest energy level. This potential induces a splitting of the degenerate 3d orbitals. Lowest in energy are the spin–orbit coupling $\lambda_r \mathbf{L}_r \cdot \mathbf{S}_r$ ($r = 2$ or 3) for each metal ion and the antiferromagnetic exchange $J_c \mathbf{S}_2 \cdot \mathbf{S}_3$ mediated by the oxalate molecules.

With matrix elements given by the overlap integrals of the crystal-field potential with the fivefold degenerate d orbitals, the crystal-field Hamiltonian of a single M(II) or M′(III) ion can be written as a 5×5 matrix [9]. Upon diagonalizing this matrix, we obtain two doublet energy levels and one singlet, with eigenvectors $|\psi_{1,2}\rangle$, $|\psi_{4,5}\rangle$ and $|\psi_3\rangle$. The orbital angular momenta of the low-lying doublets on the M(II) and M′(III) sites are given by $\pm L_2$ and $\pm L_3$: $\langle\psi_{1,2}|\mathbf{L}|\psi_{1,2}\rangle = \pm L_r \mathbf{z}$ points in the out-of-the-plane or $\mathbf{z}$ direction. Whereas the orbital angular momenta of the doublets are generally nonzero, the orbital angular momentum of the singlet vanishes. If the singlet on the M(II) or M′(III) site lies lowest in energy, we would take L_2 or L_3 equal to zero.

Within the low-energy doublets, the effective Hamiltonian for an antiferromagnetically coupled bimetallic oxalate can be written as

$$H = J_c \sum_{\langle i,j\rangle} \mathbf{S}_{2i} \cdot \mathbf{S}_{3j} + \lambda_2 \sum_i L^z_{2i} S^z_{2i} + \lambda_3 \sum_j L^z_{3j} S^z_{3j}, \quad (1)$$

where the $\langle i, j\rangle$ sum runs over all nearest neighbors, the i sum runs over all M(II) sites and the j sum runs over all M′(III) sites. The antiferromagnetic exchange J_c is positive. As discussed above, $L^z_{2i} = \pm L_2$ and $L^z_{3j} = \pm L_3$ can each take two values on the low-energy doublets.

We would like to emphasize that the orbital angular momenta of the low-energy doublets, L_2 and L_3, are modified by the crystal fields. They are not the same as the total angular momenta of the M(II) or M′(III) multiplets before the crystal field is taken into account. For example, in an octahedral crystal field (which can be obtained as a limit of the C_3-symmetric potential [10]), the orbital angular momentum L_3 of the e_g doublet for an Mn(III) ion is quenched although the $3d^4$ multiplet had $L = 2$ before it was split by the crystal field.

3. Magnetization and magnetic compensation

Mean-field (MF) theory is used to treat the exchange interaction $J_c \mathbf{S}_2 \cdot \mathbf{S}_3$ between the antiferromagnetically coupled M(II) and M′(III) spins. The MF Hamiltonians on M(II) and M′(III) sites are then

$$H_2 = \lambda_2 L^z_2 S^z_2 + 3 J_c S^z_2 \langle S^z_3\rangle \quad (2)$$

$$H_3 = \lambda_3 L^z_3 S^z_3 + 3 J_c S^z_3 \langle S^z_2\rangle. \quad (3)$$

Since equations (2) and (3) are evaluated in the subspace of the M(II) and M′(III) doublets, the energy levels ϵ_r are given by

$$\epsilon_2 = (\pm\lambda_2 L_2 + 3 J_c \langle S^z_3\rangle)\sigma_2, \quad (4)$$

$$\epsilon_3 = (\pm\lambda_3 L_3 + 3 J_c \langle S^z_2\rangle)\sigma_3, \quad (5)$$

where $\sigma_2 = S_2, S_2-1, \ldots, -S_2$ and $\sigma_3 = S_3, S_3-1, \ldots, -S_3$.

Taking $g = 2$ for both M(II) and M′(III) ions and setting $\mu_B = 1$, the magnetic moments on the M(II) and M′(III) sites are $M_2 = \langle 2S^z_2 + L_2\rangle$ and $M_3 = \langle 2S^z_3 + L_3\rangle$, which must be solved self-consistently. The average magnetization is then given by $M_{avg} = (M_2 + M_3)/2$. We adopt the convention that $M_2 > 0$ and $M_3 < 0$. Results in the next section also employ the estimate $J_c = 0.5$ meV obtained from MF theory [9]. Although a recent Monte Carlo study [12] suggests that J_c is about twice as large, our results are insensitive to the precise value of J_c, provided that it is small compared to the spin–orbit coupling.

To characterize the magnetic behavior of a bimetallic layer as a function of the crystal-field angular momenta L_2 and L_3, we make use of the limiting behavior of M_{avg} as $T \to T_c$ and $T \to 0$. In the first case

$$M_{avg} \sim \sqrt{T_c - T}, \qquad T \to T_c. \quad (6)$$

While the square-root behavior is an artifact of MF theory [12], the proportionality factor is a function of L_2 and L_3. As $T \to 0$, the ground-state magnetization depends on the signs of the spin–orbit coupling on the M(II) and M′(III) sites. The spin–orbit coupling constant λ of a $3d^n$ electronic configuration is negative when the d orbitals are more than half-filled ($n > 5$) and positive when they are less than half-filled ($n < 5$). So for electronic configurations $3d^{n_2}$ and $3d^{n_3}$ on the M(II) and M′(III) sites, the average magnetization at $T = 0$ is given by

$$M_0 = \left(S_2 + \frac{L_2}{2}\mathrm{sgn}(n_2 - 5)\right) - \left(S_3 + \frac{L_3}{2}\mathrm{sgn}(n_3 - 5)\right). \quad (7)$$

Knowing the sign of M_{avg} near T_c together with its sign at $T = 0$ allowed us to determine possible regions of MC in the parameter space of $\{L_2, L_3\}$. For example, when $M_{avg} < 0$ as

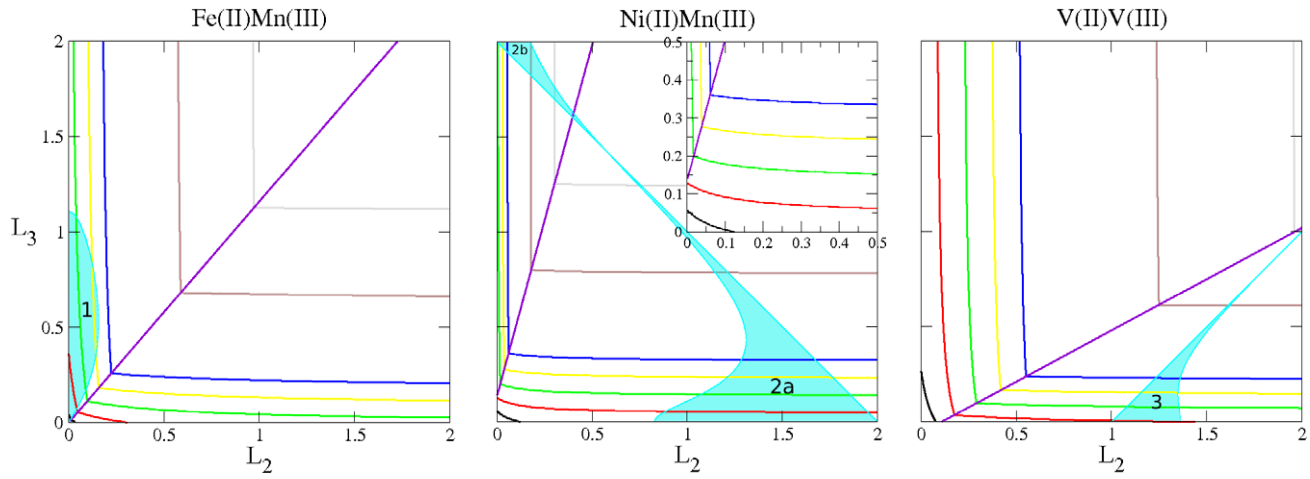

Figure 2. Contour plots of the SW gap $\Delta(L_2, L_3)$ and the associated MC region for Fe(II)Mn(III), Ni(II)Mn(III) and V(II)V(III). Each plot contains seven contours with $\Delta = 1, 2, 3, 4, 5, 10$ and 15 meV, moving out from the origin as Δ increases. The diagonal separators satisfy the condition $\Delta_+ = \Delta_-$.

$T \to T_c$ and $M_0 > 0$ then the sublattice magnetizations change from $|M_3| > |M_2|$ above T_{comp} to $|M_2| > |M_3|$ below T_{comp}.

Regions of MC are presented in figure 2 for the three compounds M(II)Mn(III) (M = Fe and Ni) and V(II)V(III). The prominent features that distinguish the MC regions are the shapes of their boundaries. For Ni(II)Mn(III) and V(II)V(III), the MC regions have straight diagonal boundaries along which the sublattice magnetizations exactly cancel at $T = 0$. The curved boundaries represent the onset of MC at T_c. In all cases, the sublattice with the smaller magnetization at $T = 0$ initially orders faster than the sublattice with the larger magnetization at $T = 0$.

4. Spin-wave frequencies

We now calculate the SW spectrum for an antiferromagnetically coupled bimetallic oxalate. Because the spin–orbit interaction $\lambda_3 \mathbf{L}_{2i} \cdot \mathbf{S}_{2i}$ or $\lambda_3 \mathbf{L}_{3j} \cdot \mathbf{S}_{3j}$ can be replaced by $\lambda_2 L^z_{2i} S^z_{2i}$ or $\lambda_3 L^z_{3j} S^z_{3j}$ within the low-energy doublet on the M(II) or M′(III) sites, there are no $L^{\pm}_{2i}$ or $L^{\pm}_{3j}$ terms in the Hamiltonian of equation (1) that can flip the orbital angular momentum. Therefore, the crystal-field orbital angular momentum acts as an Ising variable and has no intrinsic dynamics. At low temperatures, $\langle L^z_{2i} \rangle$ and $\langle L^z_{3j} \rangle$ are almost fully saturated and can be replaced by $-\mathrm{sgn}(\lambda_2) L_2$ and $\mathrm{sgn}(\lambda_3) L_3$. So the Hamiltonian at low temperatures can be rewritten as

$$H = J_c \sum_{\langle i,j \rangle} \mathbf{S}_{2i} \cdot \mathbf{S}_{3j} - |\lambda_2| L_2 \sum_i S^z_{2i} + |\lambda_3| L_3 \sum_j S^z_{3j}. \quad (8)$$

The absolute values ensure that the energy is minimized with the convention that $\langle S^z_{2i} \rangle > 0$ and $\langle S^z_{3j} \rangle < 0$.

A Holstein–Primakoff (HP) expansion about the classical limit is performed for the Hamiltonian in equation (8). The Heisenberg operators $\mathbf{S}_{2i}$ and $\mathbf{S}_{3j}$ can be transformed into boson creation and destruction operators $a^\dagger_i, b^\dagger_j, a_i$, and b_j provided that $\langle a^\dagger_i a_i \rangle \ll S_2$ and $\langle b^\dagger_j b_j \rangle \ll S_3$. These conditions are satisfied at low temperatures and for large spins S_2 and S_3. To first order in $1/S_i$, the Heisenberg operators take the form

$$S^+_{2i} = \sqrt{2S_2}\, a_i, \quad (9)$$

$$S^+_{3j} = \sqrt{2S_3}\, b^\dagger_j, \quad (10)$$

$$S^-_{2i} = \sqrt{2S_2}\, a^\dagger_i, \quad (11)$$

$$S^-_{3j} = \sqrt{2S_3}\, b_j, \quad (12)$$

$$S^z_{2i} = S_2 - a^\dagger_i a_i, \quad (13)$$

$$S^z_{3j} = -S_3 + b^\dagger_j b_j. \quad (14)$$

Fourier-transforming equations (9)–(14) and substituting the results into equation (8), we obtain the SW Hamiltonian:

$$H^{SW} = \sum_{\mathbf{k}} \{3J_c \sqrt{S_2 S_3} (\gamma^*_{\mathbf{k}} a^\dagger_{\mathbf{k}} b^\dagger_{\mathbf{k}} + \gamma_{\mathbf{k}} a_{\mathbf{k}} b_{\mathbf{k}}) + (3J_c S_3 + |\lambda_2| L_2) a^\dagger_{\mathbf{k}} a_{\mathbf{k}} + (3J_c S_2 + |\lambda_3| L_3) b^\dagger_{\mathbf{k}} b_{\mathbf{k}}\}, \quad (15)$$

where

$$\gamma_{\mathbf{k}} = \frac{1}{3}\left\{ e^{ik_x a} + 2e^{-ik_x a/2} \cos\left(\frac{\sqrt{3}}{2} k_y a\right)\right\} \quad (16)$$

is complex with $\gamma_{\mathbf{k}} = \gamma^*_{-\mathbf{k}}$ due to the lack of inversion symmetry. Generally, the error involved in an HP expansion for spins of magnitude S at low temperatures is of the order of $1/(2S + 1)$.

An equations-of-motion technique is used to diagonalize H^{SW}. The vector

$$\underline{u}_{\mathbf{k}} = \begin{pmatrix} a_{\mathbf{k}} \\ b^\dagger_{\mathbf{k}} \end{pmatrix}, \quad (17)$$

is a solution of

$$i \frac{d\underline{u}_{\mathbf{k}}}{dt} = [\underline{u}_{\mathbf{k}}, H^{SW}] = \underline{M}\, \underline{u}_{\mathbf{k}} = \omega(\mathbf{k}) \underline{u}_{\mathbf{k}} \quad (18)$$

where $\underline{M}$ is a 2×2 matrix. This system of equations requires that $\mathrm{Det}\{\underline{M} - \omega(\mathbf{k})\underline{I}\} = 0$, which yields a pair of solutions

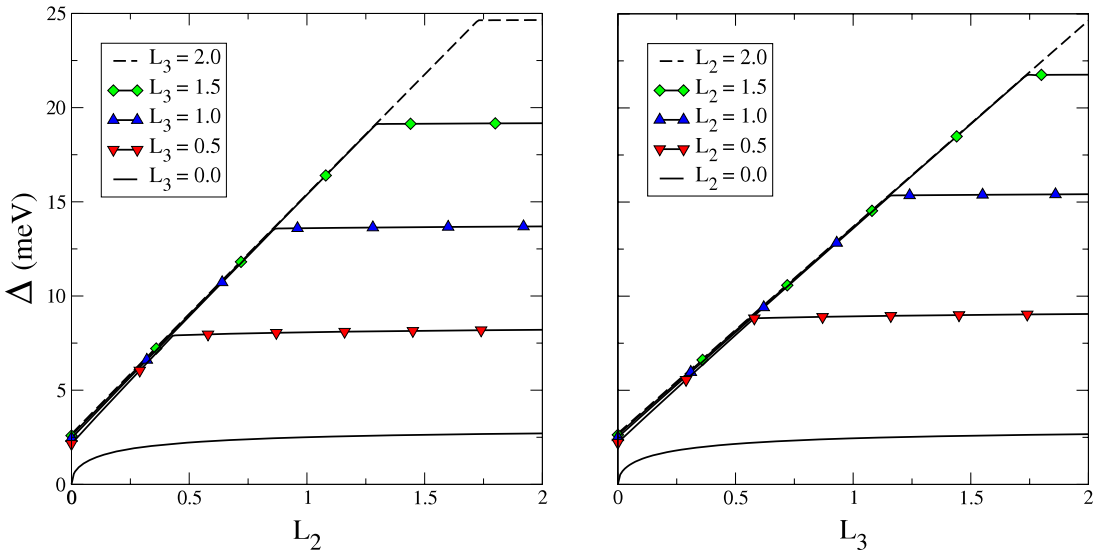

Figure 3. The SW gap Δ versus L_2 and L_3 for Fe(II)Mn(III). Fixed values of L_2 and L_3 are increased from 0 to 2 in steps of 0.5.

for $\omega(\mathbf{k})$. Replacing $\underline{u}_\mathbf{k}$ by $\underline{u}_\mathbf{k}^\dagger$ gives another pair of solutions. The four solutions to the two determinantal equations then consist of two equal and opposite pairs. We retain the two positive solutions

$$\omega^\pm(\mathbf{k}) = \pm\tfrac{1}{2}(3J_c(S_3 - S_2) + |\lambda_2|L_2 - |\lambda_3|L_3) + \tfrac{1}{2}\{(3J_c(S_2 + S_3) + |\lambda_2|L_2 + |\lambda_3|L_3)^2 - 36J_c^2|\gamma_\mathbf{k}|^2 S_2 S_3\}^{1/2}. \quad (19)$$

When $S_2 = 2$, $S_3 = 5/2$ and $\lambda_3 = 0$, this expression reduces to an earlier one [10] for the Fe(II)Fe(III) bimetallic oxalates.

At $\mathbf{k} = 0$, $\gamma_\mathbf{k} = 1$ and the SW spectrum develops a gap Δ due to the spin–orbit anisotropy. Defining the $\mathbf{k} = 0$ SW frequencies by $\Delta_\pm \equiv \omega^\pm(\mathbf{k} = 0)$, the SW gap is given by $\Delta = \min(\Delta_+, \Delta_-)$. To better appreciate the behavior of Δ as a function of L_2 and L_3, we have constructed the three contour plots in figure 2 for Fe(II)Mn(III), Ni(III)Mn(III) and V(II)V(III) compounds. The contours represent constant values of Δ in $\{L_2, L_3\}$ parameter space. It is clear that the SW gap is enhanced as $L_2, L_3 \to 2$. The contours consist of two channels, Δ_+ and Δ_-, running parallel to the L_3 and L_2 axes, respectively. Along the diagonal lines in figure 2, Δ_+ and Δ_- are equal, which is satisfied when

$$3J_c(S_3 - S_2) + |\lambda_2|L_2 - |\lambda_3|L_3 = 0. \quad (20)$$

The slope of this diagonal separator is given by $|\lambda_2/\lambda_3|$.

The result that the channels Δ_+ and Δ_- are essentially constant or parallel to the L_3 and L_2 axes, respectively, can be understood by expanding the frequencies in powers of J_c/f where $f \equiv |\lambda_2|L_2 + |\lambda_3|L_3 \gg J_c$:

$$\Delta_+ \approx |\lambda_2|L_2 + 3J_cS_3 + \vartheta\left(\frac{J_c^2}{f}\right), \quad (21)$$

$$\Delta_- \approx |\lambda_3|L_3 + 3J_cS_2 + \vartheta\left(\frac{J_c^2}{f}\right). \quad (22)$$

So to lowest order in $J_c/|\lambda_i|$, Δ_+ and Δ_- are given by $|\lambda_2|L_2$ and $|\lambda_3|L_3$, respectively, and are independent of L_3 and L_2. From equation (19), the SW gap vanishes in the limit $L_2, L_3 \to 0$, independent of the channel Δ_+ or Δ_-.

The contours $\Delta(L_2, L_3)$ of figure 2 contain seven values ranging from 1 to 15 meV. To illustrate the possible interplay between the SW gap and MC, each figure also indicates the region of MC for that compound. For Fe(II)Mn(III) compounds, the sublattice spins are identical, with $S_2 = S_3 = 2$ and the spin–orbit couplings $\lambda_2 = -12.64$ meV and $\lambda_3 = 10.91$ meV are similar in magnitude. Consequently, the first term in equation (20) vanishes and the separator terminates at the origin with slope $|\lambda_2/\lambda_3| \approx 1.15$. Notice that $\Delta \to 0$ in both the Δ_+ and Δ_- channels as $L_2, L_3 \to 0$. Because $|\lambda_2| \approx |\lambda_3|$, Δ_+ and Δ_- are evenly distributed in $\{L_2, L_3\}$ parameter space. Also notice that the MC region for Fe(II)Mn(III) overlaps the Δ_+ frequencies between 0 and 4 meV.

Another view of the contour plot for Fe(II)Mn(III) compounds is provided in figure 3, which illustrates the behavior of Δ versus L_2 and L_3. Below the kink in the left-hand or right-hand panel, $\Delta = \Delta_+$ or Δ_-; above the kink, $\Delta = \Delta_-$ or Δ_+. These plots clearly reveal the behavior of equations (21) and (22): above the kinks, Δ_- depends weakly on L_2 and Δ_+ depends weakly on L_3. The lowest curves in figure 3 indicate that $\Delta \to 0$ in both the Δ_+ and Δ_- channels as L_2 and $L_3 \to 0$.

A contour plot for Ni(II)Mn(III) compounds is shown in the center of figure 2. Unlike the case for Fe(II)Mn(III) compounds, the sublattice spins are unequal and the magnitude of the spin–orbit couplings are quite different: Ni(II) has $S_2 = 1$ and $|\lambda_2| = 40.29$ meV while Mn(III) has $S_3 = 2$ and $|\lambda_3| = 10.91$ meV. Since the first term on the right-hand side of equation (20) is nonzero, $\Delta_+ - \Delta_- \to 3J_c(S_3 - S_2) = 1.5$ meV as $L_2, L_3 \to 0$ and the separator has a slope of $|\lambda_2/\lambda_3| = 3.69$. The nonzero intersect of equation (20) with the L_3 axis allows the Δ_- channel to occupy a greater portion of the $\{L_2, L_3\}$

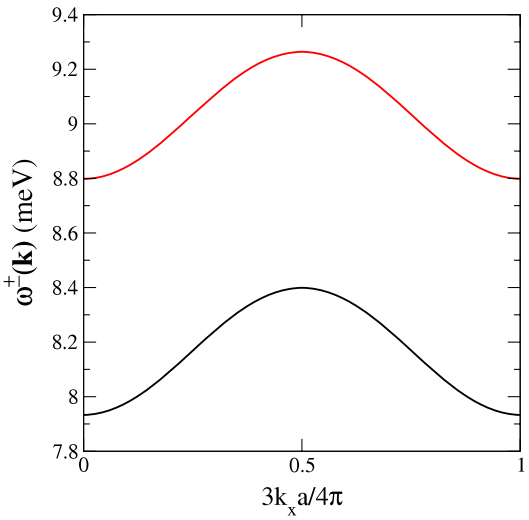

Figure 4. The SW frequencies $\omega^{\pm}(\mathbf{k})$ versus $k_x a$ for Fe(II)Mn(III) with $L_2 = L_3 = 0.5$ and $k_y = 0$.

parameter space. In the inset, we have blown up the region from $L_r = 0$ to 0.5. Notice that the contours $\Delta = 1$ and 2 meV exist only in the Δ_- channel. As the gap energy increases to 3 meV, the Δ_+ channel reappears. The two MC regions for Ni(II)Mn(III) compounds appear in figure 2. While the SW channel Δ_- traverses region 2a, Δ_+ traverses region 2b.

On the right of figure 2, the last set of contours is drawn for V(II)V(III) compounds. The V(II) and V(III) ions have spins $S_2 = 3/2$ and $S_3 = 1$, and spin–orbit coupling $\lambda_2 = 6.94$ meV and $\lambda_3 = 12.89$ meV, respectively. So $\Delta_+ - \Delta_- \to 3J_c(S_3 - S_2) = -3/4$ meV as $L_2, L_3 \to 0$. Because $S_3 < S_2$, equation (20) has a nonzero intersect with the L_2 axis. Due to the small slope $|\lambda_2/\lambda_3| = 0.53$ of the separator, the Δ_+ channel occupies the majority of parameter space. Notice that the contours in the Δ_- channel transverse the region of MC for V(II)V(III) compounds.

The SW frequencies $\omega^{\pm}(\mathbf{k})$ are plotted as a function of $k_x a$ in figure 4 for the compound Fe(II)Mn(III) with $L_2 = L_3 = 0.5$. As can easily be seen from figure 1, the wavevector of the ferrimagnetic order on the open honeycomb lattice is given by $\mathbf{Q} = (4\pi/3a)\mathbf{x}$. The maximum in the dispersion along the k_x axis occurs at $k_x = 2\pi/3a$, corresponding to a change of about 0.5 meV relative to the Γ point $\mathbf{k} = 0$. Generally, equation (19) can be expanded in powers of J_c/f to show that the width of the SW dispersion along the k_x axis is approximately $8J_c^2 S_2 S_3/f$. The difference between the two frequencies $\omega^{\pm}(\mathbf{k})$ is constant as k_x crosses the first Brillouin zone, with a value given by equation (20). The lower frequency at $\mathbf{k} = 0$ gives the SW gap Δ_-, in agreement with the Fe(II)Mn(III) contours of figure 2.

5. Conclusion

We have calculated the SW frequencies for antiferromagnetically coupled bimetallic oxalates. Our results for the SW gap were demonstrated by studying the compounds Fe(II)Mn(III), Ni(II)Mn(III) and V(II)V(III) as a function of their associated crystal-field orbital angular momentum L_2 and L_3. The SW gap varied from 0 meV to as high as 15 meV as the angular momenta L_2 and L_3 increased. There does not seem to be any relationship between the SW gap and the presence or absence of MC. Indeed, the SW gap can achieve its largest value outside regions of MC, as seen particularly in figure 2 for the Fe(II)Mn(III) compounds. These results indicate that even compounds that do not exhibit MC may have sizeable SW gaps. However, when the singlet levels on both the M(II) and M′(III) sites lie lowest in energy, then both L_2 and L_3 would vanish and MC would be absent. Since any magnetic anisotropy would then be produced by single-ion anisotropy $D_i \propto \lambda_i^2$, the SW gaps would tend to be much smaller than those predicted here.

Depending on whether Δ_+ or Δ_- is smaller, the SW gap depends primarily on the orbital angular momentum L_2 or L_3 of the M(II) or M′(III) ion, respectively. This surprising result stems from the small value of the exchange interaction J_c compared to the magnitude of the spin–orbit coupling constants λ_i.

In addition to the above compounds, we also constructed the contours $\Delta(L_2, L_3)$ for V(II)Cr(III), Co(II)Mn(III), Fe(II)Ru(III) and Cu(III)Ru(III). For the V(II)Cr(III) and Co(II)Mn(III) compounds, we found similar behavior as in figure 2. On the other hand, Ru(III) compounds with a $4d^5$ electronic configuration displayed an order-of-magnitude higher value of Δ because of the large spin–orbit coupling $\lambda_3 = 116.54$ meV and low-spin $S_3 = 1/2$ state [5].

Hopefully, this paper will inspire future measurements of the SW excitations in the bimetallic oxalates. Although almost all samples are polycrystalline, inelastic neutron scattering measurements on deuterated materials should be able to measure the SW gap without difficulty.

Acknowledgments

We would like to acknowledge helpful conversations with Drs Patrik Henelius, Juana Moreno and Fernando Reboredo. This research was sponsored by NSF grant nos DMR-0548011, OISE-0730290 and EPS-0447679 (ND EPSCoR), the Laboratory Directed Research and Development Program of Oak Ridge National Laboratory, managed by UT-Battelle, LLC for the US Department of Energy under contract no. DE-AC05-00OR22725, and by the Division of Materials Science and Engineering of the US DOE.

References

[1] Tamaki H, Zhong Z J, Matsumoto N, Kida S, Koikawa M, Achiwa N, Hashimoto Y and Ōkawa H 1992 *J. Am. Chem. Soc.* **114** 6974

[2] Bénard S, Yu P, Audière J P, Rivière E, Clément R, Guilhem J, Tchertanov L and Nakatani K 2000 *J. Am. Chem. Soc.* **122** 9444
Bénard S, Rivière E, Yu P, Nakatani K and Delouis J F 2001 *Chem. Mater.* **13** 159

[3] Coronado E, Galán-Mascarós J R, Gómez-García C J and Laukhin V 2000 *Nature* **408** 447

[4] Mathonière C, Nuttall C J, Carling S G and Day P 1996 *Inorg. Chem.* **35** 1201

[5] Larionova J, Mombelli B, Sanchiz J and Kahn O 1998 *Inorg. Chem.* **37** 679
[6] Min K S, Rhinegold A L and Miller J S 2005 *Inorg. Chem.* **44** 8433
[7] Coronado E, Galán-Mascarós J R and Martí-Fastaldo C 2006 *J. Mater. Chem.* **11** 2685
[8] Watts I D, Carling S G, Day P and Visser D 2005 *J. Phys. Chem. Solids* **66** 932
[9] Fishman R S and Reboredo F A 2007 *Phys. Rev. Lett.* **99** 217203
[10] Fishman R S and Reboredo F A 2008 *Phys. Rev.* B **77** 144421
[11] Reis P, Fishman R S, Reboredo F A and Moreno J 2008 *Phys. Rev.* B **77** 174433
[12] Henelius P and Fishman R S 2009 *Phys. Rev.* B at press (arXiv:0809.1012)